

Fast Track

Philipp Reineck
Christoph J. Wienken
Dieter Braun

Department of Physics, Systems
Biophysics, Center for
Nanoscience, Ludwig
Maximilians Universität
München, München, Germany

Received August 24, 2009
Revised October 16, 2009
Accepted October 16, 2009

Research Article

Thermophoresis of single stranded DNA

The manipulation and analysis of biomolecules in native bulk solution is highly desired; however, few methods are available. In thermophoresis, the thermal analog to electrophoresis, molecules are moved along a microscopic temperature gradient. Its theoretical foundation is still under debate, but practical applications for analytics in biology show considerable potential. Here we measured the thermophoresis of highly diluted single stranded DNA using an all-optical capillary approach. Temperature gradients were created locally by an infrared laser. The thermal depletion of oligonucleotides of between 5 and 50 bases in length were investigated by fluorescence at various salt concentrations. To a good approximation, the previously tested capacitor model describes thermophoresis: the Soret coefficient linearly depends on the Debye length and is proportional to the DNA length to the power of 0.35, dictated by the conformation-based size scaling of the diffusion coefficient. The results form the basis for quantitative DNA analytics using thermophoresis.

Keywords:

Capillary / Single stranded DNA / Thermophoresis

DOI 10.1002/elps.200900505

1 Introduction

Simple methods to analyze molecules in solution are rare but highly sought-after for molecular biology. For example, electrophoresis is still the backbone of most DNA sequencing approaches and is a reliable tool in molecular biology. Methods to analyze molecules in bulk solution are important since surface-based approaches often render proteins or even DNA dysfunctional. Molecules move along a microscopically applied temperature difference of only a few Kelvin (Fig. 1A). This effect is termed thermophoresis, thermal diffusion or the Soret effect. Thermophoresis has only recently been pursued on the biological realm [1, 2, 3]. Based on these measurements, one can expect that thermophoresis reveals information about the native interface between molecule and solvent with high sensitivity, allowing the sensitive probing of biomolecule binding (Wienken, C. J. *et al.* and Baaske, P. *et al.*, submitted). In contrast to electrophoresis, the molecules are probed in physiological buffer, in the future possibly even in such complex fluids as, for example, blood serum.

Here we present measurements for single stranded DNA and describe the results with a microscopic theory without fitting parameters. The results allow the extrapolation of

thermophoresis for similar biological molecules. Besides measuring the Soret coefficient, *i.e.* the strength of the thermophoretic effect, the diffusion coefficients of the molecules are also measured. Measurements are performed on the timescale of several minutes and are performed in sample volumes well below one microliter. We report on an optical, capillary-based technique which yields highly reproducible and sensitive results. Notably, the combination of thermophoresis and fluid flow also allows for a number of conditions in which molecules are strongly accumulated [4–8] and the thermophoretic effect is exponentially amplified.

1.1 Basics of thermophoresis

While thermophoresis bodes well for biomolecule analysis in minute sample volumes, the fundamental description of thermophoresis is the subject of a long standing debate with ongoing experimental efforts. Among others, our group has argued in the past that in the limit of diluted molecules, under interface-free optical conditions and the typically used moderate temperature gradients, the steady state of thermophoresis can be described by a local Boltzmann distribution of the particle density. In thermophoresis, unlike in electrophoresis, the particle movement is dominated by diffusion, not by the particle drift. An effective Peclet number P_e can be given by

$$P_e = a \frac{v}{D} = a \frac{D_T}{D} \nabla T = a S_T \nabla T \quad (1)$$

Correspondence: Professor Dieter Braun, Department of Physics, Systems Biophysics, Center for Nanoscience, Ludwig Maximilians Universität München, Amalienstr. 54, 80799 München, Germany

E-mail: dieter.braun@lmu.de

Fax: +49-89-2180-16558

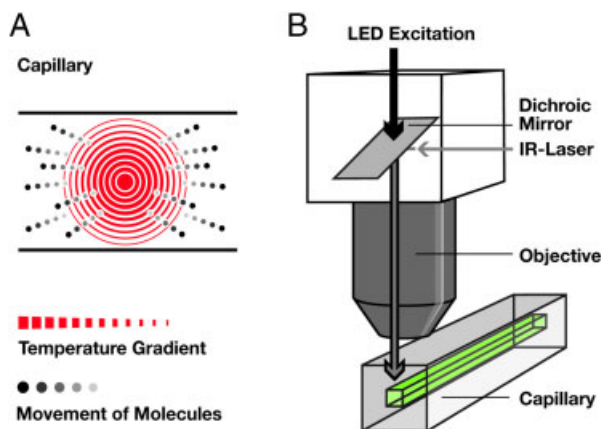


Figure 1. Thermophoresis and setup. (A) Molecules move in a temperature gradient, an effect termed thermophoresis. Typically, the movement in aqueous solutions is directed away from regions of elevated temperature. (B) We measure thermophoresis inside a rectangular capillary with a $50\ \mu\text{m} \times 50\ \mu\text{m}$ cross-section. The temperature gradient is applied locally on the micrometer scale by an infrared laser. The concentration of the molecules is monitored with a fluorescent tag on the molecule. The temperature distribution in the capillary is measured in a separate measurement utilizing a temperature-sensitive fluorescent dye.

with particle radius a , particle drift velocity v , diffusion coefficient D , thermophoretic mobility D_T , Soret coefficient S_T and the temperature gradient ∇T . The diffusive movement of single molecules allows the reversible equilibration between particle positions due to temperature differences in the Gibbs free enthalpy of the molecule-solvent complex [1, 9–13]. This results in a steady-state molecule distribution which is given by a linear thermophoretic drift $v = -D_T \nabla T$ and the backdiffusion flux $j = -D \nabla c$ with diffusion coefficient D . Only under the condition $P_e \gg 1$, which is experimentally challenging to achieve even for micrometer-sized particles, we could experimentally confirm a local fluid flow of solvent around the molecules [14]. The Soret coefficient is defined as the ratio $S_T = D_T/D$ and determines the magnitude of thermodiffusion in steady state. With above assumptions, it is given by the temperature derivative of the Gibbs free energy G of the molecule-solvent complex [1, 15]:

$$S_T = \frac{1}{k_B T} \frac{\partial G}{\partial T} \quad (2)$$

This approach was previously tested with polystyrene beads with varying particle size, salt concentration and temperature and for the case of double stranded DNA with varying length. The results were described quantitatively without fitting parameters [1]. Further confirmation of the approach was found from the study of quartz beads [16]. Extensions of the theory were reported in [17]. Subsequent experiments on polystyrene beads [18] came to different conclusions concerning the size dependence. Results obtained using an electrical heating grid remained inconclusive [19]. It should however be mentioned that the use of interfaces to apply the temperature

gradient as used in [18, 19] could allow for the buildup of electrical fields which in turn leads to the rather complex coupling of thermophoresis and electrophoresis [20]. On the other hand, we expect that optical application of the temperature difference used in our study (Fig. 1B) strongly reduces such buildup of “thermoelectrophoresis” due to the lack of an interface layer which can be charged. Test measurements were unable to confirm the influence of electrical fields in our experimental settings (unpublished results).

While it is difficult to precisely chemically modify the surface of polystyrene beads in a way that the modification is independent of particle size, DNA is a highly defined and characterized molecule. DNA is biologically highly relevant and gives us a defined length and molecule characteristics. We measured single stranded DNA from 5 to 50 bases in length. Double stranded DNA was measured previously in a length range above the persistence length of double stranded DNA, namely between 50 and 50000 base pairs. As before, we used a length range where the polymer length and diameter yields approximately a spherical molecule geometry. Previously, the measurements were restricted to comparably low salt concentrations due to indications of DNA sticking to the used planar chambers. The capillaries used here show considerably less surface interactions and well-defined washing steps after the measurement allow the precise quantification of sticking. Overall, the approach allowed us now to test theoretical predictions for polymers other than double stranded DNA.

The manuscript is structured as follows: we describe the capillary-based measurement procedure, check the validity of the used theoretical modeling of the measurement, report on the measured Soret and diffusion coefficients and describe the measurements with a microscopic theory of double layer energies.

2 Materials and methods

2.1 Setup and measurement chambers

A modified fluorescence microscope shown schematically in Fig. 1 has been utilized to obtain temperature and concentration distributions in solution. The IR laser enters the setup laterally between microscope body and objective, is deflected by a rotatable dichroic mirror and is focused in the sample plane by the objective. The cube containing the dichroic mirror is mounted on a AxioTech Vario fluorescence microscope (Zeiss, Oberkochen, Germany). Fluorescence excitation is provided by a high performance LED (Luxeon, Calgary, Canada). The emission light is recorded by a Sencam QE CCD camera (PCO, Kehlheim, Germany). Capillaries are made of fused silica with a square cross-section and an inner diameter of $50 \times 50\ \mu\text{m}$ (Polymicro Technologies, Phoenix, AZ, USA) and used as microfluidic measurement chambers. Inner dimensions vary only by $\pm 0.5\ \mu\text{m}$ per 10 m capillary length which significantly

enhances the reproducibility of temperature profiles generated in solution. Capillaries were filled by placing the sample solution in a micro test tube on one end of the capillary while air pressure was reduced slightly at the other end using a syringe. Subsequently, both ends were sealed with mineral oil in order to prevent the sample from evaporating. Pressure differences are allowed to equilibrate for at least 30 s to reduce undesired drift in the capillary. Only 250 nL sample volume is needed to fill a capillary of 10 cm length. Binding of molecules to the capillary surface is low and was tested by measuring residual fluorescence after rinsing the capillary with buffer. Experimental error for S_T measurements is $\pm 0.0021/K$ due to noise of the fluorescence signal in addition to a relative error of ± 2.3 to $\pm 4\%$ which accounts for the precision of the temperature measurements. Diffusion constants are determined with an accuracy of ± 10 to $\pm 20\%$ since depletion kinetics of simulations match measured traces equally well within this range.

2.2 Infrared heating

Temperature gradients in solution were generated locally by the absorption of an infrared laser (Fibotec Fiberoptics Meiningen, Germany) at a wavelength of 1450 nm. At this wavelength water strongly absorbs with an absorption length of 320 μm . The collimated IR laser beam was focused in the sample plane by the microscope objective (Fig. 1). Temperature differences created in solution ranged between 2.3 and 4.4 K. These were measured utilizing the temperature dependence of the fluorescent dye Cy5 (carboxymethyl-indocyanine-*N*-dyroxysuccinimidyl ester) in $1 \times \text{SSC}$, which was determined independently. Temperature differences in capillaries were reproducibly generated and measured with a precision of ± 0.1 K. This error is estimated from the noise present in the spatially resolved fluorescence signal and from the precision with which the IR laser can be positioned in the center of the capillary.

2.3 Molecules

Single stranded DNA of 5, 10, 22 and 50 bases (Biomers, Ulm, Germany) were diluted to $1 \mu\text{M}$ and investigated at different salt concentrations. The following sequences were used:

5-mer: 5'-Hex-TA GTT-3' 10-mer: 5'-Hex-TA GTT CTA AT-3'; 22-mer: 5'-Hex-AT TGA GAT ACA CAT TAG AAC TA-3' 50-mer: 5'-Hex-ATAATCTGTAGTACTGCAGA AAAC TTGTGGGTTACTGTTTACTATGGGGT-3'.

The solution was buffered with 1 mM Tris at pH 7.6. The Debye length was titrated with KCl according to

$$\lambda_{\text{DH}} = \sqrt{\frac{\varepsilon_0 \varepsilon_r k_B T}{2 N_A e^2 (c_S + c_T)}} \quad (3)$$

where ε_0 is permittivity of free space, ε_r the dielectric constant of water, $k_B T$ the thermal energy, N_A is Avogadro's number, e the elementary charge and c_S and c_T are concentration of KCl and Tris, respectively. All oligonucleotides were labeled with HEX (-carboxy-2',4,4',5',7,7'-hexachlorofluorescein) at the 5' end.

2.4 Measurements

Under typical measurement conditions, DNA moves against temperature gradients in solution. Therefore, in a region of elevated temperature, the DNA concentration decreases. If the molecules are fluorescently labeled this can be imaged by a local decrease in fluorescence intensity (Fig. 2). As shown in Fig. 3, this signal is evaluated over time in the heating center for a typical measurement: the infrared laser is turned on at time $t = 10$ s and turned off again after 240 s. During this time the temperature distribution in the solution is in steady state. As the molecules move away

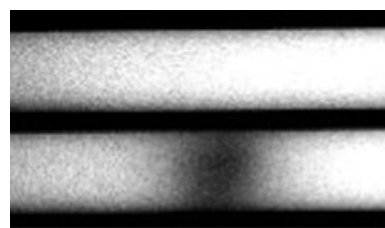


Figure 2. Microscopy of capillary fluorescence. Fluorescence images of the capillary containing labeled DNA before (top) and after (below) the temperature gradient is applied. Fluorescence decreases due to particles moving away from the hot spot.

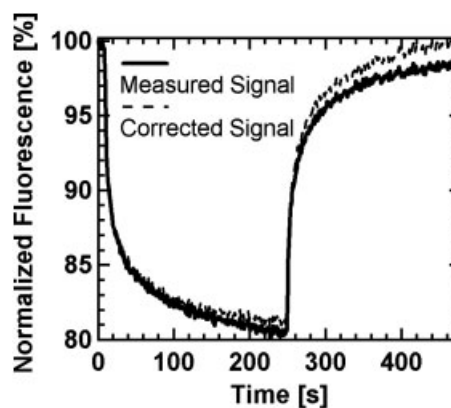


Figure 3. Time trace and bleaching. Normalized fluorescence in the heating center evaluated over time. At time $t = 10$ s a temperature gradient is applied and molecules move away from the hot spot as seen from the decrease of the fluorescence signal. Molecules diffuse back after the IR laser is turned off at $t = 250$ s. The signal does not fully recover due to bleaching (solid line). This artifact can be corrected for with high precision (dashed line).

from the hot spot, the concentration initially decreases exponentially. As soon as the IR laser is turned off, molecules freely diffuse back to a uniform concentration distribution. Due to low excitation intensities, bleaching artifacts are small and can be corrected precisely by fitting the change in fluorescence intensity from unheated regions of the capillary. Two quantities can be obtained from a measurement over time. The Stokes–Einstein diffusion constant D from the kinetics of the depletion dynamics and the Soret coefficient S_T from the magnitude of the depleted concentration.

2.5 Analyzing the measurements

1-D, 2-D and 3-D models of the measurement geometry and timing were created and evaluated utilizing finite element simulations (Femlab, Comsol, Stockholm, Sweden). The 1-D model represents a radially symmetric, two dimensional circular plane with a diameter of $800\ \mu\text{m}$ in which the heating center and the center of the circle coincide. The 2-D and 3-D model are $800\ \mu\text{m}$ in length as well but respect the capillary boundaries and are $50\ \mu\text{m}$ wide (2-D and 3-D) and $50\ \mu\text{m}$ in height (3-D). This way the influence of capillary geometry and convection (only 3-D) on the temporal evolution of diffusion processes were investigated. Heat transport through the capillary walls was included by the measured temperature profile. For numerical reasons, the concentration was held constant at the long ends of the capillary. Due to its distance to the heating center, back diffusion from the boundary did not affect the simulation. The flux equation accounting for diffusion and thermodiffusion is $\vec{j} = -D_T c \nabla T - D \nabla c$. We apply the continuity equation and add the term $\nabla(\vec{v}c)$ to introduce convection for the case of the 3-D simulation. The fluid velocity \vec{v} is obtained by solving the Navier–Stokes equation. Therefore, we solved the time dependent partial differential equation $\partial c / \partial t = \nabla(D_T c \nabla T + D \nabla c) - \nabla(\vec{v}c)$. The temperature profile T was turned on and off instantaneously with heavy-side functions $\Theta(t) = \Theta_1(t - t_1)\Theta_2(t_2 - t)$ due to the negligible thermal relaxation time in the millisecond regime. As the temperature is turned on at t_1 and turned off at t_2 the whole measurement procedure was simulated.

To compare different simulation models, we idealized a typical temperature distribution by a Gaussian profile with a width of $\sigma = 27\ \mu\text{m}$ and a peak temperature difference of 2.3 K. Other constants were chosen typical for the largest measured 50-mer single stranded DNA molecule with $D = 56\ \mu\text{m}^2/\text{s}$ and $D_T = 5.6\ \mu\text{m}^2/\text{sK}$ where measurement artifacts from thermal convection are expected to be maximal. The simulated time lines are shown in Fig. 4A. To probe thermal convection, the 3-D simulation was executed with and without gravity acting on the fluid. Maximum convection velocities emerged in the proximity of the focused IR laser $v_x = 77\ \text{nm/s}$ and $v_z = 131\ \text{nm/s}$ (Fig. 4B) and were found to have no significant influence on the thermophoretic concentration depletion in steady state ($<0.57\%$).

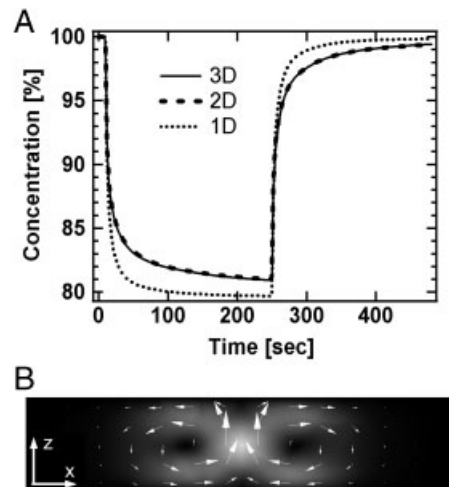


Figure 4. Simulation of thermophoretic depletion. (A) Simulation of the measurement process for the different model geometries, evaluated in the heating center. The 1-D model deviates from the 2-D and 3-D models significantly. (B) Side view of the 3-D simulation of the capillary. Maximum convection velocities occur in the heating center (center of the image) are $v_x = 77\ \text{nm/s}$ and $v_z = 131\ \text{nm/s}$ and are indicated by the arrows. Results of the 2-D and 3D models are hardly distinguishable and show that the influence of convection is negligible.

To understand this deviation, we calculated the Peclet number $P_e = L \cdot u / D$, now applied on the scale of the measurement chamber. Its value determines whether a fluid system is dominated by diffusion or by the movement of the fluid. Here, $L = 27\ \mu\text{m}$ is the characteristic length of the system, $u = 130\ \text{nm/s}$ the velocity of the fluid due to convection and D the diffusion constant of the solved particles. For the slowest diffusing particle in our experiments, 50-mer single stranded DNA molecules, the Peclet number is calculated to $P_e = 0.063$. Since the convection flow is anti-parallel to the thermophoretic outward drift at the chamber bottom and parallel at its top, deviations are likely to perturb the concentration profile in second order of the convection velocity. Indeed, the squared Peclet number ($P_e^2 = 0.40\%$) comes close the simulated deviations (0.57%). Overall, this indicates a clear domination of diffusive transport over the convective fluid flow.

However, the effect of the restricted capillary geometry on the temporal evolution of the model is significant and shown in Fig. 4A. Even though diffusion constants are identical, depletion kinetics in the spatially unrestricted 1-D model are much faster and the diffusion and the thermodiffusion fluxes almost fully equilibrate, *i.e.* at $t = 240\ \text{s}$ the 1-D simulation is very close to steady state while the concentration in the other models still decreases. Since the 2-D and 3-D simulations show rather small deviations of the depleted concentration, the 2-D model was chosen as the basis for the evaluation of measurements.

For comparison, we also evaluated analytical solutions to the diffusion equation. According to [21, 22] the axial diffusion equation under a Gaussian perturbation shows a central

concentration over time which can be approximated by

$$c(t, \tau, c_0, c_\infty) = c_\infty + c_0 \left(1 - \sum_{i=0}^{\infty} \frac{(-K)^i}{i![(2t/\tau + 1)i + 1]} \right) \approx \frac{c_0 + c_\infty(t/\tau)}{1 + t/\tau} \quad (4)$$

with the starting concentration c_0 , the final concentration c_∞ and the diffusive relaxation time $\tau = \sigma^2/D$ with the width σ of the Gaussian temperature profile and diffusion coefficient D . For the series expansion, the constant K is defined by the zero of $(1 - e^{-K})/K = c_\infty/c_0$. We use the formula for both the thermophoretic depletion and the backdiffusion by choosing appropriate starting and final conditions c_0 and c_∞ . Due to the symmetry between thermal and mass diffusion, the heating and cooling kinetics can be modeled by the same equation according to $c \rightarrow T$ with a thermal relaxation time $\tau \rightarrow \tau_{\text{thermal}}$, approximated to $\tau_{\text{thermal}} = d^2/\kappa$ with the thermal diffusivity κ and the chamber thickness d . We can infer the fluorescence signal using the bleaching correction with time constant τ_{bleach} , the temperature dependence of the dye $\alpha = \partial F/\partial T$ and both the heating and cooling time points t_H , t_C . The laser is switched on with a step function $h(t) = \theta(t - t_H) * \theta(t_C - t)$, backdiffusion is timed by $b(t) = \theta(t - t_C)$ and the initial time before depletion switched on with $i(t) = \theta(t_H - t)$ where $\theta(t)$ defines Heavy-side functions. The depletion dynamics of concentration is given by $c_{\text{DEPL}}(t) = c(t - t_H, \tau, 1, e^{-\alpha T})$ with a temperature sensitive fluorescence given by the thermal relaxation $T_{\text{HEAT}}(t - t_H, \tau_{\text{thermal}}, 1, 1 + \alpha \Delta T)$. Likewise the back diffusion dynamics is modeled by $c_{\text{DIFF}}(t) = c \times (t - t_C, \tau, c_{\text{DEPL}}(t_C - t_H), 1)$ under a cooling dynamics of $T_{\text{COOL}}(t - t_C, \tau_{\text{thermal}}, 1 + \alpha \Delta T, 1)$. Since thermal diffusivity is typically 100–1000 times faster, we can assume $\tau \gg \tau_{\text{thermal}}$ and superpose the thermal and mass diffusion dynamics by separating the time scales. With the initial fluorescence F_0 and the bleaching dynamics, the measured fluorescence then becomes:

$$F(t) = [c_{\text{DEPL}}(t)T_{\text{HEAT}}(t)h(t) + c_{\text{DIFF}}(t)T_{\text{COOL}}(t)b(t) + i(t)]F_0e^{-t/\tau_{\text{bleach}}} \quad (5)$$

As expected, the analytical solution does not differ from the one-dimensional finite element solution under Gaussian heating. However, the common deviations of the thermal profile from the Gaussian shape render the above analytical treatment only an approximation. Also, it is restricted to the dynamics in the heating center, not the fluorescence surrounding of the heated spot which is often used to check the details of the diffusion dynamics. Notably, the same criticism concerning the applicability of the 1-D finite element solution in confined capillary geometries applies (Fig. 4A). However for fast fitting purposes, the approach has its validity.

The real temperature profile as measured by fluorescence is neither exactly Gaussian nor Lorentzian. Hence, it was important to independently quantify the temperature distribution with a spacial resolution below 1.5 μm (Section 2). The profile is incorporated into the model as a

fitted polynomial of the order of 15, which allowed sufficient precision (<1%) to describe the temperature profile in both shape and magnitude.

The recorded fluorescence images were analyzed by Labview routines (National Instruments, Austin, TX, USA). All images were normalized to the first ten images where no temperature gradient is present. The resulting signal is thereby corrected against minor illumination inhomogeneities of the microscope. The temperature dependence of the fluorescence of the dye is determined in independent measurements using the temperature controlled Peltier stage and was found to be small (0.0%/K–0.24%/K). This value varies for different DNA length and salt concentrations and affects the measurement only slightly; however, it was determined independently for every measurement condition. We correct for this by subtracting the temperature dependence on a pixel-by-pixel basis according to the temperature distribution present in solution. This is carried out 100 ms after the IR laser is turned on since simulations have shown that at this time the temperature gradient is equilibrated throughout the capillary while the thermophoresis of the temperature dye itself is not yet significant [23, 24]. Photobleaching results in an exponential decay of fluorescence signal over time and is accounted for by dividing the signal by $\exp(t/\tau)$, where t is time and τ is the characteristic timescale of bleaching which is fitted. As a result, we can infer the DNA concentration from the fluorescence intensity. This trace of DNA concentration over time can be directly compared with simulated time traces.

Numerical evaluation of the model was carried out on the basis of Matlab (MathWorks, Natick, MA, USA). The model structure, together with the solving algorithms, for the differential equations was provided by Femlab. Simulated and measured time lines were compared using a Labview program. Here, the traces of DNA concentration over time obtained from the fluorescence signal were compared with theoretical time traces from FEMLab simulations using sample specific parameters provided by the Labview routine. The only fitted parameters were the Soret coefficient S_T and the diffusion constant D . By varying both, the simulated time lines were fitted to the measured time lines. In Fig. 5A the result of this process is shown for time lines obtained for different positions along the capillary, starting at the heating center, going outward parallel to the capillary walls. Simulated and measured temporal evolutions of relative concentration of DNA at different positions in the capillary are in good agreement. As would be expected, the thermophoretic depletion is strongest in proximity of the heating center ($x = 3 \mu\text{m}$) and becomes smaller as distance increases ($x = 20 \mu\text{m}$). The temporary increase in concentration at large distances from the center ($x = 60 \mu\text{m}$) originates from molecules moving away from the hot spot, an effect which is more prominent in the confined capillary geometry as compared with previously used two dimensional fluid films [1, 11]. Likewise, the evaluation of the concentration distributions along the capillary axis at given times shows good agreement between theory and measurement (Fig. 5B). Besides selected spatial and

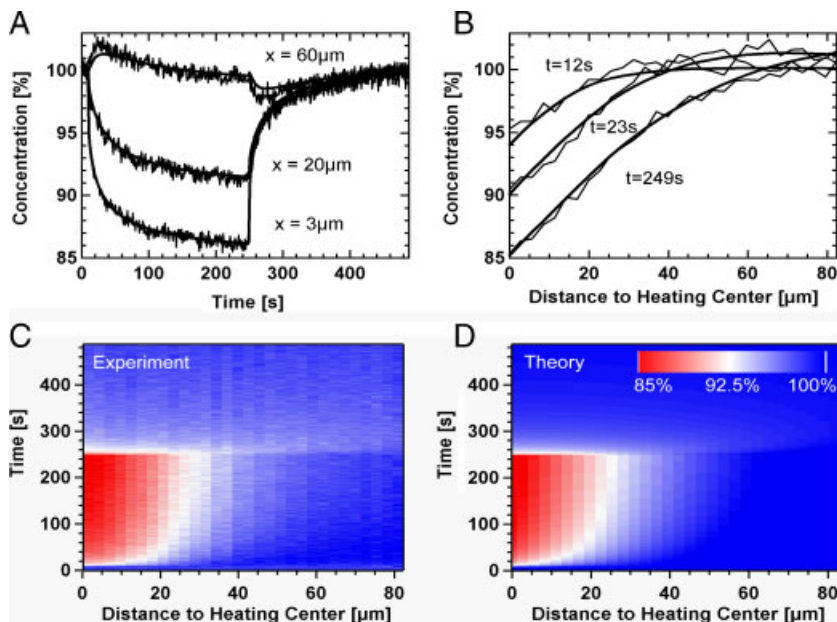


Figure 5. Thermophoresis in experiment and theory. Comparison of measurements and simulations for a 50-base Single stranded DNA molecule at a Debye length of $\lambda_{\text{DH}} = 3.7$ nm. (A) Change of the concentration over time is evaluated at different positions along the capillary. (B) Concentration profiles parallel to the capillary at its center at specific times are well described by the simulated concentration profiles using the 2-D model. (C, D) The concentration in a space–time plot of the thermophoretic depletion is represented by colors. The experimental space–time (C) is well described by the theoretical space–time (D). Note that the information represented in (A) and (B) are vertical and horizontal cross sections of the space–time plot at fixed values of distance or time, respectively.

temporal cross sections, we can also visualize the concentration in a space–time graph, demonstrating the fine agreement between measurements (Fig. 5C) and simulations (Fig. 5D) for all measured times and distances.

3 Results and discussion

The Soret coefficient of single stranded DNA molecules of 5, 10, 22 and 50 bases length, diluted to a concentration of $1 \mu\text{M}$, was measured in solution as a function of salt concentration. The Debye shielding length is inversely proportional to the square root of salt concentration. The solution was buffered with 1 mM Tris at pH 7.6. Salt concentrations in the range between 2 and 500 mM KCl were investigated. This range corresponds to Debye shielding lengths of 5.6 and 0.43 nm, respectively. Values for D and S_T were obtained by fitting the measured data in a spacial-temporal manner as shown in Fig. 5. Soret coefficients scale linearly with Debye length for all molecules with a small intercept at $\lambda_{\text{DH}} = 0$ (Fig. 6A). The diffusion constant decreases with increasing oligonucleotide length and is well fitted by a power law $D \sim (\text{bases})^{-0.45}$ (Fig. 6B).

The Soret coefficient of double stranded DNA down to a length of 50 bases has been previously derived as

$$S_T = \frac{A}{k_B T} \frac{\beta \sigma_{\text{eff}}^2}{4\epsilon\epsilon_0 T} \lambda_{\text{DH}} + S_T^{\text{off}} \quad (6)$$

without free parameters [1]. Here, $\sigma_{\text{eff}} = Q_{\text{eff}}/A$ is the effective charge *per* surface area and ϵ and ϵ_0 the permittivity of water and free space, respectively. The parameter β contains the temperature dependence of both the permit-

tivity of water [25] and the Debye length: $\beta = 1/(T\epsilon)(d\epsilon/dT)$. The central term is the entropy of ionic shielding and is calculated from the temperature derivative of the Gibbs Free Enthalpy of the ionic shielding for thin Debye layers $G_{\text{ionic}} = Q_{\text{eff}}^2 \lambda_{\text{DH}} / 2(\epsilon\epsilon_0 A)$. In a simplified picture, this contribution can be interpreted as electrical energy stored in a capacitor consisting of the molecule's surface charges on the one side, separated against the shielding ions in solution on the other side.

The offset value S_T^{off} will be fixed when evaluating the experiments. It includes from a theoretical perspective a size independent “ideal gas” contribution $S_T^B = 1/T$ that stems from work against the osmotic pressure [11]. However, its contribution is rather small ($S_T^B = 0.0034 \text{ K}^{-1}$) and should contribute only significantly for small molecules measured at large salt concentrations. Another contribution to the offset is the hydrophobic interaction with water. It is expected to be salt independent for the comparably low salt concentrations in our experiments and is modeled by $-A s_{\text{hyd}}/k_B T$ where s_{hyd} is the hydration entropy *per* molecule surface area A and $k_B T$ the thermal energy. It accounts for the change in water structure due to the presence of the single stranded DNA molecules, including, for example, the creation of the water cavity for the molecule and the hydrophobic interactions at its interface. In principle, we could separate the “ideal gas” contribution from contributions stemming from s_{hyd} by size dependent measurements of the offset in a $S_T(\lambda_{\text{DH}})$ plots. However experimental errors prevent such analysis at least in the measurements presented here.

Based on electrophoresis measurements, the effective charge of single stranded DNA is about $0.5e/\text{base}$ [26–28], considerably higher than the value for double stranded DNA. The theory of counterion condensation predicts an effective

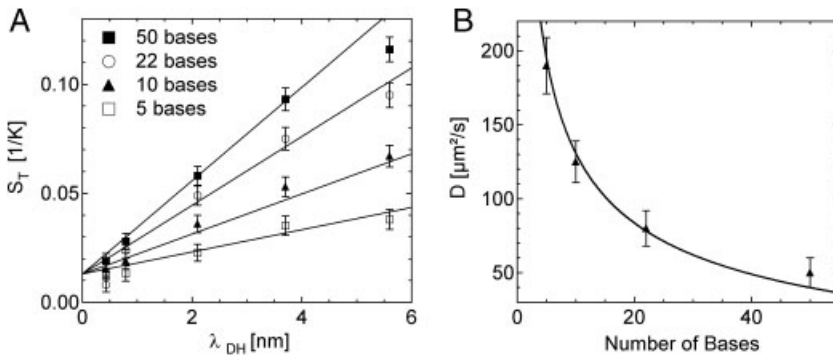


Figure 6. Salt dependence. (A) The Soret coefficient S_T versus Debye length for single stranded DNA ranging from 5 to 50 bases in length. The linear increase is quantitatively described by Eq. (6) with $Q_{\text{eff}} = 0.5e/\text{base}$ without fitting parameters other than the comparably small offset at zero Debye length. (B) Diffusion coefficients for the DNA molecules obtained from the same measurement. Values are well fitted with a power law $D \sim \text{bases}^{-0.45}$.

charge of $0.6e/\text{base}$ for single stranded DNA [29, 30]. These values do not depend on salt concentration in the range investigated here and were shown to be largely temperature insensitive. The surface area of the molecules was approximated to be spherical with a radius inferred from the measured diffusion coefficients according to the Stokes–Einstein relation $r = k_B T / (6\pi\eta D)$. Measurements performed on longer single stranded DNA fragments (280–5386 bases) yields a persistence length ranging from 1 to 5 nm for salt concentrations in the 10^{-1} to the 10^{-3} M regime [31, 32]. Assuming a polymer length of 1.5 nm for the 5-mer, the persistence length is longer than polymer length for most measurements. But given a width of about 1 nm for single stranded DNA, a spherical approximation is still feasible. One should note that for the measurements under low salt and short DNA, we are at the boundary of the applicable range of Eq. (6), working rather in the regime $R \geq \lambda_{\text{DH}}$ than strictly under $R \gg \lambda_{\text{DH}}$ necessary for the capacity model. Nevertheless, the theory describes the behavior of short Single stranded DNA molecules quite well.

As shown in Fig. 6A, the linear increase of S_T for single stranded DNA is described well by Eq. (6). Besides an offset of $S_T^{\text{off}} = 0.013\text{K}^{-1}$, no fitting parameters were used and the Soret coefficients were described microscopically from first principles. The offset is comparably small and probably of complex origin and nature. For single stranded DNA, a free fit of the offset shows no systematic dependence on the DNA length. In previous experiments using polystyrene beads with considerably larger Soret coefficients, a similar offset was found which however scaled – within experimental errors – with the particle surface [1]. For each measurement point, the measured diffusion coefficient was used to infer the molecule size. Similar to polystyrene beads, the linear dependence on the Debye thickness is not only confirmed but also predicted quantitatively from a microscopic picture of charge screening.

The change of the salt concentration did not systematically change the size of the ssDNA molecules in the measured salt range and allowed the direct linear plot of the

Soret coefficient based on Eq. (6). The measured diffusion coefficients are shown in Fig. 6B and are in fair agreement with literature values [31, 32] considering that for short single stranded DNA the fluorescent label cannot be neglected and will result in a slightly reduced diffusion coefficient. Diffusion constants are fitted with a power function. Including a minor offset we find D proportional to $L^{-0.45}$ with L denoting the number of bases.

It follows from the results of Fig. 6A that the length dependence of the thermophoresis of single stranded DNA should be predictable as well. Starting with a fixed offset $S_T^{\text{off}} = 0.013\text{K}^{-1}$ and interpolating the diffusion coefficient from the power law fit of Fig. 6B, we can directly infer the length dependence of the Soret coefficient without introducing additional external parameters (Fig. 7). We see that the measured Soret coefficients are fairly well predicted by Eq. (6) as a function of DNA length at various salt concentrations.

To demonstrate the potential of thermophoresis for highly sensitive length discrimination, let us consider the difference between a 25-mer and a 26-mer of single stranded DNA. The difference in their respective Soret coefficients ΔS_T can be approximated from the total differential of Eq. (6). By using the dependence $A \propto D^{-2}$ and $Q_{\text{eff}} = A\sigma_{\text{eff}}$ together with differences in the charge ΔQ_{eff} and the diffusion coefficient ΔD we get:

$$\Delta S_T / S_T = 2\Delta Q_{\text{eff}} / Q_{\text{eff}} + 2\Delta D / D. \quad (7)$$

With a change $\Delta D / D = -0.028$ inferred from Fig. 6B and $\Delta Q_{\text{eff}} / Q_{\text{eff}} = 1/25$ we can expect a relative change of the Soret coefficient of $\Delta S_T / S_T = 0.024$. Measurements of the Soret coefficient with a comparably low error can be achieved. Single nucleotide resolution was shown utilizing a calibration curve approach (Wienken, C. J. *et al.*, submitted). High-resolution thermophoresis was also used to monitor the binding of a single ATP to the DNA (Baaske, P. *et al.*, submitted). We expect applications of the technique where an exact length determination of short DNA molecules is sought-after, *e.g.* for detecting short tandem repeats or single nucleotide polymorphisms in DNA analytics.

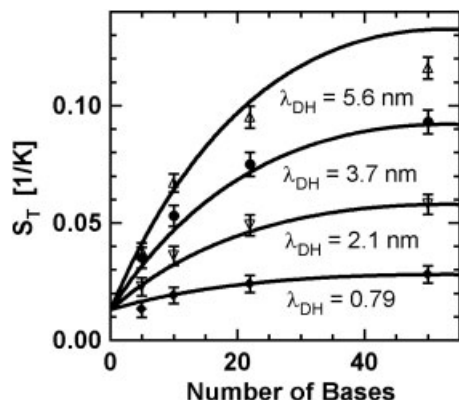


Figure 7. Length dependence. The Soret coefficient as a function of DNA length calculated from Eq. (6) with the interpolated diffusion coefficient obtained from Fig. 6B. The measured S_T values match well the theoretical expectations for various salt concentrations, indicated by the respective Debye lengths.

4 Concluding remarks

Capillaries are found to be highly reliable and non-sticky microfluidic environments for the optical investigation of thermophoresis in solution. Only small sample volumes (<250 nL) are required while the experiments are highly reproducible due to the well-defined chamber geometry of the capillaries. The thermophoretic depletion of single stranded DNA, driven by a local increase in temperature of only a few Kelvins, is monitored by fluorescence in detail and well described by 2-D simulations. As a side effect diffusion coefficients of the molecules are obtained from the experiments. Interestingly, the microscopic theory of thermophoresis based on a local thermodynamic equilibrium describes the thermophoresis of single stranded DNA – besides a small and expected offset – without fitting parameters. We find the expected linear dependence of the Soret coefficient on the Debye length without free parameters. At all considered salt concentrations the dependence of the Soret coefficient on DNA length is highly predictable.

The authors thank Ricky Dunbar and Franz Weinert for proofreading the manuscript and Inga Tegtmeier for creating Figs. 1A and B. Further we thank NanoTemper Technologies GmbH for fruitful discussions concerning the experimental setup. We also thank for the support from the Emmy-Noether Program of the Deutsche Forschungsgemeinschaft, the LMU Innovative Initiative on Functional NanoSystems (FUNS), the Excellence Cluster NanoSystems Initiative Munich (NIM) and the Center for Nanoscience (CeNS).

The authors have declared no conflict of interest.

5 References

- [1] Duhr, S., Braun, D., *Proc. Natl. Acad. Sci. USA* 2006, 103, 19678–19682.
- [2] Braun, D., Libchaber, A., *Phys. Rev. Lett.* 2002, 89, 188103.
- [3] Iacopini, S., Piazza, R., *Europhys. Lett.* 2003, 63, 247–253.
- [4] Clusius, K., Dickel, G., *Naturwissenschaften* 1938, 26, 546.
- [5] Debye, P., *Ann. Phys.* 1939, 36, 284–294.
- [6] Braun, D., Libchaber, A., *Phys. Rev. Lett.* 2002, 89, 188103.
- [7] Duhr, S., Braun, D., *Phys. Rev. Lett.* 2006, 97, 038103.
- [8] Baaske, P., Weinert, F. M., Duhr, S., Lemke, K. H., Russell, M. J., Braun, D., *Proc. Natl. Acad. Sci. USA* 2007, 104, 9346–9351.
- [9] Dhont, J. K. G., *J. Chem. Phys.* 2004, 120, 1632.
- [10] Dhont, J. K. G., *J. Chem. Phys.* 2004, 120, 1642.
- [11] Dhont, J. K. G., Wiegand, S., Duhr, S., Braun, D., *Langmuir* 2007, 23, 1674–1683.
- [12] Astumian, R. D., *Proc. Natl. Acad. Sci. USA* 2007, 104, 3–4.
- [13] Astumian, R. D., *J. Chem. Phys.* 2007, 126, 111102.
- [14] Weinert, F. M., Braun, D., *Phys. Rev. Lett.* 2008, 101, 164501.
- [15] Duhr, S., Braun, D., *Phys. Rev. Lett.* 2006, 96, 168301.
- [16] Ning, H., Buitenhuis, J., Dhont, J. K. G., Wiegand, S., *J. Chem. Phys.* 2006, 125, 204911.
- [17] Dhont, J. K. G., Briels, W. J., *Eur. Phys. J.* 2008, 25, 61–76.
- [18] Piazza, R., Vigolo, D., Braibanti, M., *Phys. Rev. Lett.* 2008, 100, 108303.
- [19] Putnam, S. A., Cahill, D. G., *Langmuir* 2005, 21, 5317–5323.
- [20] Würger, A., *Phys. Rev. Lett.* 2008, 101, 108302.
- [21] Yguerabide, J., Schmidt, J. A., Yguerabide, E. E., *Biophys. J.* 1982, 39, 69–75.
- [22] Axelrod, D., Koppel, D. E., Schlessinger, J., Elson, E., Webb, A. W., *Biophys. J.* 1976, 16, 1055–1069.
- [23] Baaske, P., Duhr, S., Braun, D., *Appl. Phys. Lett.* 2007, 91, 133901.
- [24] Cordero, M. L., Verneuil, E., Gallaire, F., Baroud, C. N., *Phys. Rev. E* 2009, 79, 011201.
- [25] Hill, N. E., *J. Phys. C* 1969, 3, 238–239.
- [26] Michalet, X., *Nano Lett.* 2001, 1, 341–343.
- [27] Shen, G., Tercero, N., Gaspar, M. A., Varughese, B., Shepard, K., Levicky, R., *J. Am. Chem. Soc.* 2006, 128, 8427–8433.
- [28] Stigter, D., *Biophys. J.* 1995, 69, 380–388.
- [29] Record, M. T., Anderson, C. F., Lohman, T. M., *Quart. Rev. Biophys.* 1978, 11, 103178.
- [30] Manning, G. S., *Q. Rev. Biophys.* 1978, 11, 179–246.
- [31] Nkodo, A. E., Garnier, J. M., Tinland, B., Ren, H. J., Desruisseaux, C., McCormick, L. C., Drouin, G., Slater, G. W., *Electrophoresis* 2001, 22, 2424–2432.
- [32] Tinland, B., Pluen, A., Sturm, J., Weill, G., *Macromolecules* 1997, 30, 5763–5765.